Article

Understanding the Relation between Structural and Spectral Properties of Light-Harvesting Complex II

Souloke Sen, Vincenzo Mascoli, Nicoletta Liguori, Roberta Croce, and Lucas Visscher*

Read Online

ACCESS | 📊 Metrics & More | 📖 Article Recommendations | 🆂🅸 Supporting Information

ABSTRACT: Light-harvesting complex II (LHCII) is a pigment−protein complex present in higher plants and green algae. LHCII represents the main site of light absorption, and its role is to transfer the excitation energy toward the photosynthetic reaction centers, where primary energy conversion reactions take place. The optical properties of LHCII are known to depend on protein conformation. However, the relation between the structural and spectroscopic properties of the pigments is not fully understood yet. In this respect, previous classical molecular dynamics simulations of LHCII in a model membrane [*Sci. Rep.* **2015**, 5, 1−10] have shown that the configuration and excitonic coupling of a chlorophyll (Chl) dimer functioning as the main terminal emitter of the complex are particularly sensitive to conformational changes. Here, we use quantum chemistry calculations to investigate in greater detail the effect of pigment−pigment interactions on the excited-state landscape. While most previous studies have used a local picture in which electrons are localized on single pigments, here we achieve a more accurate description of the Chl dimer by adopting a supramolecular picture where time-dependent density functional theory is applied to the whole system at once. Our results show that specific dimer configurations characterized by shorter inter-pigment distances can result in a sizable intensity decrease (up to 36%) of the Chl absorption bands in the visible spectral region. Such a decrease can be predicted only when accounting for Chl−Chl charge-transfer excitations, which is possible using the above-mentioned supramolecular approach. The charge-transfer character of the excitations is quantified by two types of analyses: one focusing on the composition of the excitations and the other directly on the observable total absorption intensities.
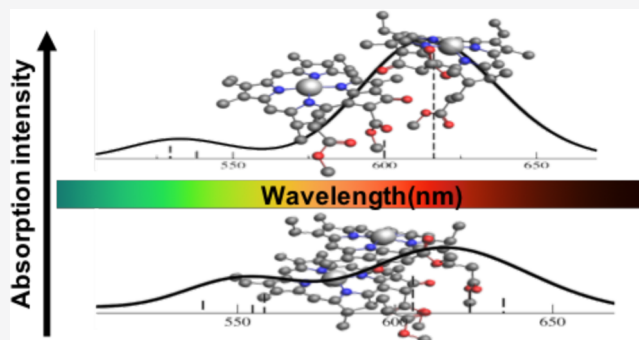
INTRODUCTION

In photosynthesis, the major light-harvesting complex II (LHCII) serves as the principal solar energy collector transferring the sunlight energy toward the reaction center of the photosystems.[1] LHCII is located in the thylakoid membrane of the chloroplast, normally presenting a trimer structure with each monomer unit binding a total of 18 pigments: six chlorophylls *b* (Chlb), eight chlorophylls *a* (Chla), and four carotenoid (Car) molecules.[2] These chromophores are responsible for sunlight absorption and are grouped into Chl−Chl and/or Chl−Car clusters according to the intensity of their excitonic interactions, given their relative orientation and proximity in space.[§] In order to understand the correlation between the conformational changes of the protein−chromophore system and the spectral properties of the complex, the inclusion of dynamical effects becomes increasingly necessary.[3] The advent of classical molecular dynamics simulations in the microsecond (μs) timescale allows probing the chromophore dynamics at an atomistic resolution, also allowing the inclusion of lipid membrane and solvent effects.[4] Snapshots from these long simulations can be used as an input for quantum chemical calculations to provide a computationally efficient strategy for

studying spectral properties of LHCs over such timescales. We note that care has to be taken that the force field reproduces the structure of the chromophores well enough[5] and have checked that the difference of excitation energies between MM and QM optimized structures does not exceed 0.1 eV. For the molecular dynamics, we build on an earlier work, where some of us have performed classical dynamics in the lipid-embedded form of LHCII.[6] Here, it was shown that the Chla611−Chla612 dimer experiences a strong deviation of the interaction energy with respect to its crystal structure. Specifically, the N-terminus movements have been found to correlate with the changes in the network of interactions around Chla612, increasing in some cases the Coulomb coupling with Chla611.[7]
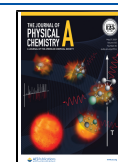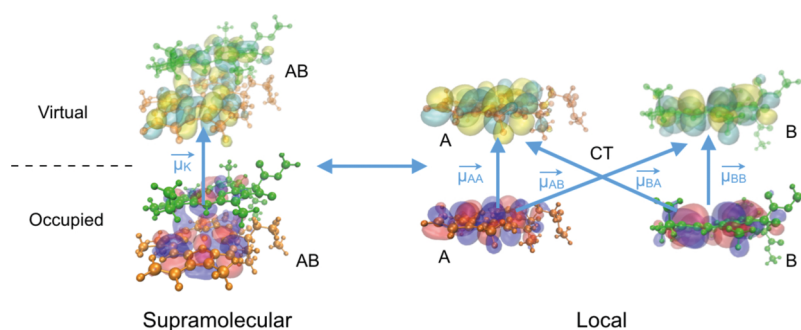
Figure 1. Conceptual diagram of an excitation of a generic AB pair of Chls in the supramolecular and local pictures. The transition dipole moments printed in the blue font are those of eqs 9 and 10.

The main purpose of the current work is to provide more detailed insights into the spectral properties of the Chla611−Chla612 pair in a set of different conformations of LHCII. Using quantum chemistry calculations based on density functional theory (DFT)[8,9] and its time-dependent extension (TDDFT),[10,11] we will be focused on the visible absorption spectrum of the Chl pair, highlighting differences between different configurations of the dimer. Our aim is to provide observables that could be experimentally measured and assist in the re-design and re-tuning of the absorption spectrum of Chl-binding complexes from the detailed knowledge of this specific pair. Our work is also of relevance for other studies on pigment−protein complexes as we demonstrate how small protein conformational changes can lead to large variations in the spectroscopic properties of the pigments.

METHODS

We use time-dependent DFT (TDDFT) in the linear response regime[10,11] to calculate the lowest eight excitations of the Chla611−Chla612 pair in a set of selected frames from two classical trajectories of solubilized LHCII. In these TDDFT calculations, the protein environment is not taken into account. All calculations are carried out with the Amsterdam Density Functional (ADF) code[12−14] using the range-separated CAMY-B3LYP exchange and correlation (XC) functional, combined with a double-zeta polarized (DZP) basis set. The details about the assessment of the CAMY-B3LYP XC functional can be found elsewhere.[7]

The trajectories belong to our previous work[6] in which we investigated a monomer of LHCII embedded in a model membrane via molecular dynamics using the GROMACS package[15] (see the Supporting Information for details on the molecular dynamics simulations). According to the original nomenclature,[6] we choose the trajectories "C" and "A" (with time lengths of 921.2 and 1036.0 ns, respectively), in which the Chla611−Chla612 dimer undergoes markedly different dynamics. From the trajectories, a total of 103 frames is selected and separated into two groups, 51 frames belonging to the beginning of the simulation and 52 frames from the end. Separation is set to 400 ps in both sets of frames. Using this sampling, we can easily compare the visible absorption of the solubilized Chla611−Chla612 pair to the one of its crystal forms, that is, by simply comparing the absorption of the last frames versus that of the initial frames. We use the VMD visualization program[16] to select and save the relevant coordinates in each frame and the RDKit library[17] to saturate the bonds with missing hydrogen atoms. The cutting of the phytol chains of the Chls and the automatization of the

calculations is done by means of Python library QMFlows[18,19] and the PLAMS[20] library interfaced with the ADF.

Local and Supramolecular Pictures. The visible absorption of a generic AB molecule can be viewed from two different perspectives (see Figure 1). The first one is a supramolecular viewpoint, in which the dimer is considered as a single unit and the electrons are delocalized over the two molecules. This picture arises naturally from the canonical Kohn−Sham orbitals as these tend to be delocalized. In the second perspective, the local picture (drawn to the right in Figure 1), the dimer is considered as formed by two individual molecules interacting with each other. Here, orbitals are considered localized on each separate molecule, no matter how close the two molecules are. This is possible because for non-covalently bonded subsystems, one may recombine the canonical occupied and virtual orbitals into well-localized ones without changing the nature of the wave functions and its energy.[21] We can use this local orbital picture to define localized Chla611 and Chla612 excitations even if the pair is a strongly interacting dimer at a short intermolecular distance. In a graphical manner, Figure 1 shows the transformation of an AB → AB supramolecular excitation to a local picture where it is decomposed into four local contributions: A → A, B → B, A → B, and B → A. The first two terms represent the neutral excitations localized on the respective monomers, while the last two terms involve occupied and virtual orbitals of different molecules, normally referred to as charge-transfer excitations. Linear combination of these four states then helps us recover the supramolecular picture. In the following, Chla611 will be interchangeably referred to as molecule A and Chla612 as molecule B.

In principle, the supramolecular and local pictures must yield the same excited-state landscape since they are just different perspectives of the same physical phenomenon. In practice, however, local models are more often used since they allow a gradual increase of the intermolecular interaction, moving smoothly from isolated molecules to the fully interacting situation. In addition, one may introduce approximations to avoid the costly supramolecular calculation. In our case, where we are interested in studying the excitations of the Chla611−Chla612 pair, we will compare the performance of the following models with an increasing level of interaction (and, therefore, accuracy):

(i) Isolated molecules model. Based on the local picture, this model represents a completely uncoupled model where the TDDFT linear response calculations are performed considering each Chla of the pair at a time. The visible absorption of the whole pair will be

estimated by the simple addition of the two isolated Chla contributions.

(ii) Uncoupled frozen density embedding (FDEu)[22,23] model. This model is based on DFT calculations in the local picture, where the Chla611−Chla612 pair is partitioned into two subsystems each corresponding to one Chla. The ground-state density of a given molecule is optimized in the presence of the other molecule that is kept as *frozen*, that is, its electrons do not explicitly enter into the Kohn−Sham procedure[9] but are present as an effective potential instead. Particularly, in our case, we use the PW91k kinetic energy,[24] the Becke88 exchange,[25] and LYP correlation[26] approximants as the additional non-additive counterparts of the regular intra-subsystem functionals, as required in the conventional formulation of subsystem DFT[27] and its extension to the TDDFT regime.[28]

In a similar way to the previous model, we can obtain the visible spectrum of the Chla611−Chla612 pair by simply adding the two individual FDEu−TDDFT Chla absorption bands. In this case, however, the FDEu approach includes the chromophore−chromophore interactions, allowing each Chla electron density to be polarized by the presence of the other. Nevertheless, similar to the previous one, this model is expected to fail when the two chromophores are close enough to induce significant coupling between the excitations.

(iii) Coupled FDE model using the Tamm−Dancoff approximation (FDEc-TDA).[28,29] Based on the combination of the FDEu approximation with TDDFT[30] (FDEu-TDDFT), the FDEc-TDA model couples the lowest subsystem excitations coming from FDEu-TDDFT calculations of the single Chls to retrieve the electronic spectrum of the total system (thus constructing a supramolecular picture). This procedure is computationally much more efficient than a full supramolecular calculation and is demonstrated to work well in the weak coupling regime, where orbitals (and electrons) remain substantially localized on each molecule. This method only accounts for neutral excited states, which can possibly be delocalized over the two molecules. The results are the so-called Frenkel exciton states, corresponding to linear combinations of the localized excitations only, i.e., A → A and B → B. However, since the molecular orbitals (MOs) remain localized, the charge-transfer contributions, that is, A → B and B → A excitations, are still missing compared to the full supramolecular treatment. The contribution of charge-transfer excitations (requiring the use of a supramolecular picture) in the description to low-lying excited states might become significant when the two chromophores are sufficiently close to each other. We note, however, that recent studies by Neugebauer and co-workers using projection-based embedding techniques (as an alternative to the conventional non-additive functionals used here) in combination with a supramolecular basis set in the context of subsystem TDDFT have been shown to be able to describe inter-subsystem charge-transfer excitations and reproduce the supramolecular results exactly.[31−34] We have not considered this extension of FDE here.

(iv) Supramolecular model. This is computationally the most demanding and, in principle, also the most accurate. In our work, we perform supramolecular TDDFT linear response calculations where the atoms of both Chla611 and Chla612 are taken into account. This is the most complete picture where in addition to the Frenkel states, the charge-transfer states are also taken into account explicitly.

In order to connect the two (local and supramolecular) pictures and provide more insights into the nature of the excitations, two complementary analysis tools are used to decompose the supramolecular excitations in terms of local excitations. First, we briefly describe the charge-transfer analysis based on the study by Plasser and Lischka[35] as implemented in the ADF code. After this, we also present a dedicated intensity decomposition scheme to express the supramolecular excitations in terms of local excitations.

Charge-Transfer Analysis. In the charge-transfer analysis proposed by Plasser and Lischka,[35] the charge-transfer number Ω_{AB}^{k} for a given excitation k is defined in terms of the transition density matrix $\mathbf{D}^{0k}$ in the basis of fragment (localized) MOs

$$\Omega_{AB}^{k} = \frac{1}{2} \left\| \mathbf{D}^{0k,AB} \right\|_{F}^{2} \tag{1}$$

where $\|\mathbf{M}\|_{F}$ is the Frobenius norm of a matrix $\mathbf{M}$. The sub-block $\mathbf{D}^{0k,AB}$ of the total MO transition density matrix $\mathbf{D}^{0k}$ is defined as

$$
\begin{aligned}
D_{ai}^{0k,AB} &= D_{ai}^{0k} && \{i \in A \wedge a \in B\} \\
D_{ai}^{0k,AB} &= 0 && \{i \ni A \vee a \ni B\}
\end{aligned}
\tag{2}
$$

In practice, it is easier to carry out the analysis in the non-orthogonal basis of atomic orbitals (AOs) with a Mayer[36] population analysis

$$\Omega_{AB}^{k} = \frac{1}{2} \left\| (\mathbf{P}^{0k} \circ \mathbf{S})^{AB} \right\|_{F}^{2} \tag{3}$$

in which the Hadamard product $(\mathbf{P}^{0k} \circ \mathbf{S})$ of the transition density $\mathbf{P}^{0k}$ and overlap $\mathbf{S}$ matrices in the AO basis appears. The sub-blocks are defined as before using the perfectly localized AOs.

Intensity Analysis. Complementary to the charge-transfer analysis is to consider the physically observable absorption of visible light directly. Given a generic AB molecule and a set of (supra)molecular excitations $\{E_1, E_2 ... E_k\}$ (where E_k represents the energy of the kth supramolecular excitation), the corresponding oscillator strengths are, in the dipole length formulation, given by the following equation (in a.u.)

$$f_k = \frac{2}{3} E_k |\vec{\mu}_k|^2 \tag{4}$$

where $\vec{\mu}_k$ is the transition dipole moment vector of the kth supramolecular excitation. In the MO basis, this dipole vector is written as

$$\vec{\mu}_k = \sum_{i}^{\text{Occ}} \sum_{a}^{\text{Virt}} D_{ai}^{k} \vec{\mu}_{ia} \tag{5}$$

with the individual matrix elements $\vec{\mu}_{ia}$ in eq 5 given as

$$\vec{\mu}_{ia} = \int \psi_a(r) \hat{r} \psi_i(r) \, d\vec{r} \tag{6}$$

where $\hat{r}$ is the position operator. In the same fashion as the CT analysis, we can switch to a local picture of the intensity by transforming to the AO basis. The transition dipole vectors are
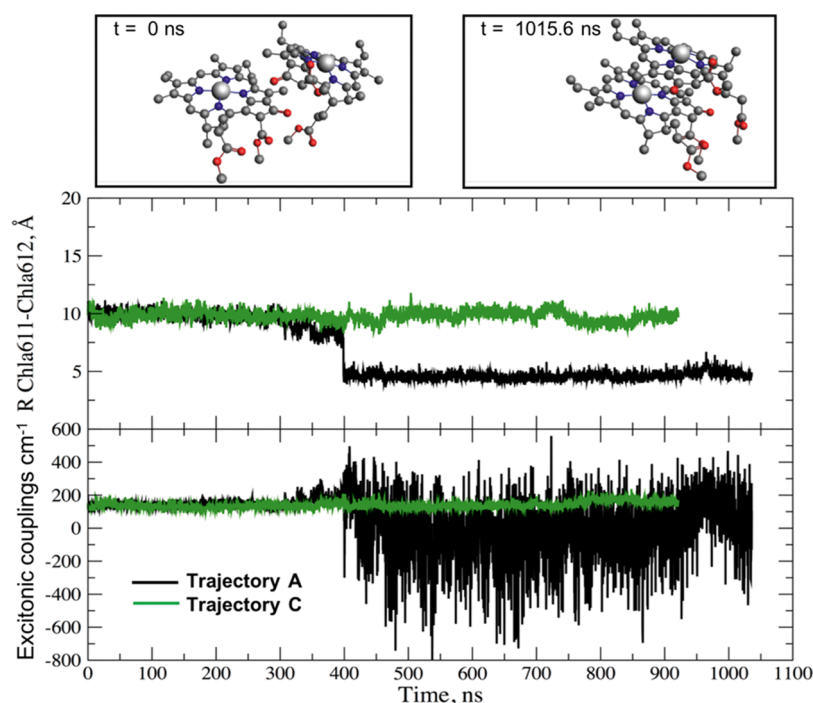
Figure 2. Inter-molecular distance and the excitonic coupling energy (in cm^{-1}) of the Chla611−Chla612 pair in the two selected classical trajectories. The upper boxes show two snapshots of the Chl−Chl dimer conformations representative of the beginning (left) and the end (right) of the trajectory "A".

then expressed in terms of the AO transition density matrix $\mathbf{P}^{0k}$ and the dipole matrix $\vec{\mathbf{M}}$

$$\vec{\mu}_k = \sum_{\kappa,\lambda}^{AOs} P_{\kappa\lambda}^{0k} \vec{M}_{\kappa\lambda} \qquad (7)$$

By defining transition density sub-blocks corresponding to the A and B parts of the AB molecule, we can then write the dipole moment vectors as a sum of the four transition dipole components previously displayed in Figure 1 and separate the contributions to the transition dipole in terms of local and charge-transfer excitations

$$\vec{\mu}_k = \vec{\mu}_k^{LE} + \vec{\mu}_k^{CT} \qquad (8)$$

$$\vec{\mu}_k^{LE} = \vec{\mu}_k^{AA} + \vec{\mu}_k^{BB} \qquad (9)$$

$$\vec{\mu}_k^{CT} = \vec{\mu}_k^{AB} + \vec{\mu}_k^{BA} \qquad (10)$$

with

$$\vec{\mu}_k^{XY} = \sum_{\kappa \in X, \lambda \in Y}^{AOs} P_{\kappa\lambda}^{0k} \vec{M}_{\kappa\lambda} \qquad (11)$$

Inserting eq 8 into eq 4 then yields

$$f_k = \frac{2}{3} E_k [|\vec{\mu}_k^{LE}|^2 + |\vec{\mu}_k^{CT}|^2 + 2\vec{\mu}_k^{LE} \cdot \vec{\mu}_k^{CT}]$$

$$= f_k^{LE} + f_k^{CT} + f_k^{OR} \qquad (12)$$

The first two terms are always positive, while the third orientation (OR) term can become negative depending on the angle between the local-excitation and charge-transfer contributions to the total transition dipole moment.

RESULTS AND DISCUSSION

Using TDDFT linear response calculations, we evaluate the visible absorption of the Chla611−Chla612 pair in two classical trajectories of LHCII (the trajectories "C" and "A", according to the original nomenclature[6]). For each of these two trajectories, we carry out TDDFT calculations on two sets of ~50 frames taken from the beginning and the end of the simulation, hereafter referred to as the first and last sets of frames (see the Methods section for details). We choose these two specific trajectories because they are characterized by markedly different dynamics of the Chla611−Chla612 dimer. In the trajectory "C", the two Chls keep an almost constant orientation and center-to-center distance (≈10 Å) throughout the dynamics, while in the trajectory "A", the two Chls become more stacked and come closer together (a center-to-center distance of ≈5 Å, see Figure 2). This difference is also reflected in the average absolute excitonic couplings of the two Q_y Chl bands that rise with the shortening distance toward the end of the trajectory "A" (Figure 2, lower panel). Additionally, in Figure 2, large fluctuations of the couplings [computed in the ideal dipole approximation $(IDA)^{6,7}$] are observed toward the end of this trajectory, resulting from a more disordered domain involving the Chl pair and the N-terminus of the protein, as reported previously by Liguori and co-workers in ref 6.

We are interested in investigating how these markedly different dimer configurations impact the absorption spectrum of the Chl pair, as predicted by a supramolecular TDDFT approach. In the following, we will analyze the results of these calculations using the supramolecular and local pictures introduced earlier.

Since the Q_y region (corresponding to the lowest-energy electronic transitions) is the most interesting to investigate and given that the reliability of TDDFT calculations in the UV region is less good,[37,38] we focus only on the wavelength range
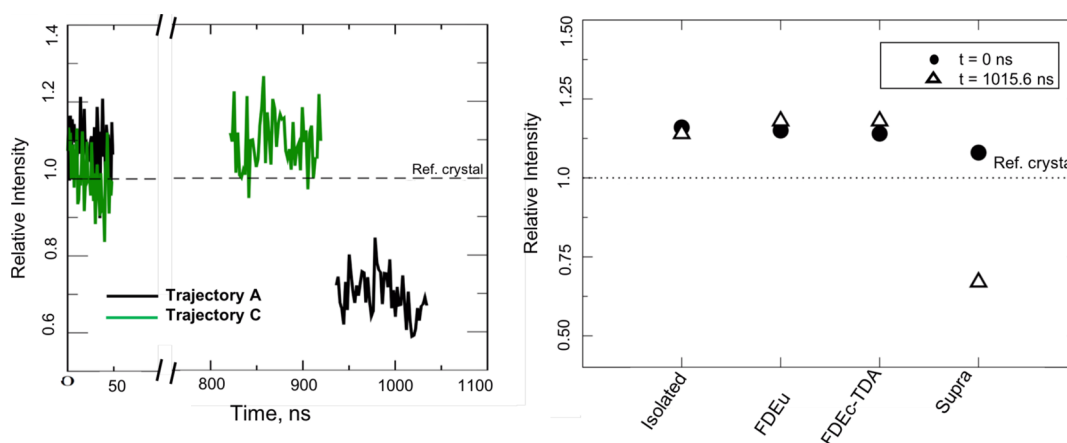
Figure 3. Left panel, Relative integrated supramolecular absorption of the Chla611–Chla612 pair in the Q-band region (using a Gaussian broadening of σ = 0.1 eV) of the selected frames of the trajectory "A" (black) and the trajectory "C" (green) with respect to the LHCII crystal structure. Left and right sides of the split on the x-axis represent the first and last set of frames from the trajectories. Right panel, Relative absorption of two selected snapshots from the beginning (filled circle) and end (bold triangle) of trajectory "A" using the different models.

from 500 to 700 nm, which falls in the green-to-red region of the visible spectrum and covers the entire Q-band region (Q_x and Q_y). This so-called Q-band region can be described sufficiently well with a CAMY-B3LYP type exchange–correlation functional. As the lowest excited states computed with TDDFT may mix among each other, we will consider the summed intensity of all states that fall in this 500–700 nm window. More specifically, integrating the entire Q region is more informative about the contribution/relevance of CT states because the excitonic interactions [which are already present in model (iii)] can possibly redistribute the intensity over the Q states but conserve the total intensity, whereas mixing with a CT state also impacts the total intensity of the Q band (besides that of specific states).

Visible Absorption of the Chla611–Chla612 Pair. In Figure 3, we plot the total Q-band absorption intensity of the Chla611–Chla612 pair for the trajectories "C" and "A" as compared to a reference value computed for the absorption of the pair in the LHCII crystal structure. As displayed in the left panel of Figure 3, the supramolecular model [model (iv) in the previous section] predicts for the Q-band intensity a substantial drop toward the end of the simulation "A", going from a relative value of 1.08 to 0.69 (averaged over the first and last set of frames of the trajectory, respectively). This corresponds to an average decrease of 36% of the initial intensity. In the right-side panel of Figure 3, we compare the performances of the different models presented in the previous section on two selected snapshots from the beginning and the end of the trajectory "A" [see Figure S1 in the Supporting Information for the averaged values for models (ii), (iii), and (iv)]. While all three approximate models based on the local picture are in good agreement with the supramolecular model in the case of the initial structure, they similarly fail to reproduce the intensity drop predicted by the supramolecular calculations for the final structure. These differences between the models indicate the possible importance of charge-transfer contributions in the supramolecular calculations as this is lacking in all the other approximate models based on a local picture. As expected, the relevance of charge-transfer contributions to the low-lying excited states is higher when the pigments are closer and more strongly interacting. For sufficiently distant pigments, the differences between the models are reasonably small, and the approximate models [i.e.,

models (i)–(iii)] then offer a computationally more efficient approach in comparison to the full supramolecular calculations.[28,29]

Supramolecular and Local Perspectives. To elucidate the cause of the intensity decrease observed at the end of the trajectory "A", we will now consider the individual excitations in the supramolecular and local pictures. We label the two lowest excitations of the dimer as Q_y and Q_y', with Q_y taken as the excitation with the lowest transition energy. In columns #3 to #5 of Table 1, the averaged excitation wavelength ($\bar{\lambda}$),

Table 1. Average Excitation energy ($\bar{E}$) in eV, Wavelength ($\bar{\lambda}$) in nm, Absorption Intensity ($\bar{f}$), and Transition Dipole Moment ($\bar{\mu}$) in debye of the Two Lowest Excitations of the Chla611–Chla612 Pair of the Trajectory "A"

frames	$\bar{E}$	$\bar{\lambda}$	$\bar{f}$	$\bar{\mu}$
		Q_y		
first set	1.98	626	0.443	7.66
last set	1.93	642	0.082	3.29
		Q_y'		
first set	2.04	608	0.094	3.35
last set	2.00	620	0.165	4.49

intensity ($\bar{f}$), and transition dipole moment ($\bar{\mu}$) of both excitations (Q_y and Q_y') in the selected first and last sets of frames of the trajectory "A" are shown. As we can see, the lowest excitation is in the last set of frames, red-shifted by about 16 nm as compared to that of the first set of frames, whereas the other excitation is red-shifted by 12 nm. This is most likely an effect of the larger mixing of the locally excited (LE) states with one or more charge-transfer (CT) states due to the shorter inter-pigment distances in the last set of frames. The red-shifted absorption caused by the increased coupling between LE and CT states is consistent with previous experiments and theoretical modeling.[39–41] Besides red-shifting, the two lowest transitions also change their oscillator strength, which steeply drops for the lowest Q_y excitation and slightly increases for the Q_y' transition at the end of the trajectory "A".

The different degree of mixing between LE and CT states is likely a consequence of the changing extent of electron delocalization over the two molecules. The latter depends on
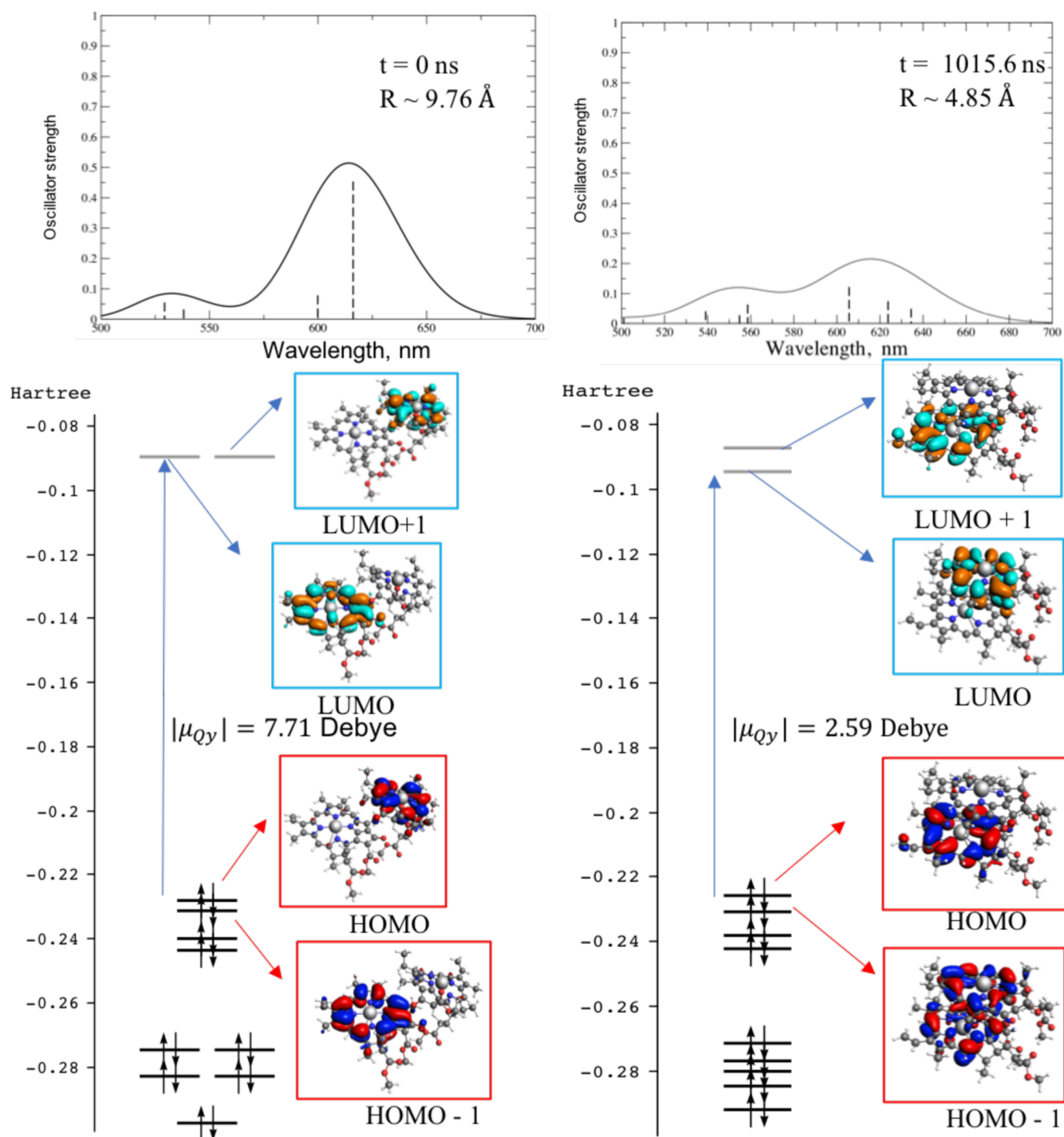
Figure 4. Upper two panels, Electronic spectra of the Chla611−Chla612 pair taken at two snapshots from the beginning (left) and the end (right) of the trajectory "A". The Gaussian broadening factor used to draw the spectra is $\sigma = 0.1$ eV. Bottom figures, MO diagrams with the HOMO and HOMO − 1 orbitals drawn in red and blue in the red squares, respectively, and the LUMO and LUMO + 1 orbitals drawn in orange and green in the blue squares, respectively. The isovalue of the orbital representations is set to 0.03 a.u. The indicated transition dipole moment value corresponds to the lowest excitation in both snapshots.

the configuration of the dimer and, particularly, on the distance between Chls, as can be recognized by looking at the orbitals involved in the lowest energy transitions. In Figure 4, we display the supramolecular orbitals of the pair, taking two snapshots of the trajectory from the beginning (left) and the end (right) of the simulation. The left side of the figure corresponds to the beginning of the trajectory where the two molecules are still far away from each other at 9.76 Å. In this

frame, the orbitals involved in the lowest excitations (Q_y and Q_y') are almost fully localized, and we can clearly identify the molecule to which they belong. The situation is different when the molecular separation is reduced to ≈4.85 Å distance. The electron delocalization increases and, as shown in the right-hand side of the orbital diagram of Figure 4, the HOMO − 1 orbital is now spread over the two porphyrin rings. At the same time, the transition dipole moment of the lowest excitation is

strongly reduced and, consequently, the absorption intensity as well (see eq 4, assuming almost constant E_k).

In order to have a more quantitative analysis of the cause of the intensity drop, we switch to a local picture. At the beginning of the simulation, the relevant canonical orbitals are fully localized on each Chl, and supramolecular TDDFT yields two excitations that can be easily identified as a linear combination of two local excitations. However, toward the end of the trajectory, the Kohn–Sham orbitals are delocalized, and the LE states are strongly mixed with the CT states. Such coupling of CT states with low-lying excitonic or Frenkel states has been observed previously in experiments,[40,42] supported by theory,[41] and reproduced with quantum chemical calculations using diabatization techniques to separate the LE states from the CT states.[31,43−45] Furthermore, it has been shown that the CT mixing in these states is substantiated by the large excitonic-phonon coupling measured in fluorescence.[39]

To quantify the average CT character of Q-band excitations independent of the nature of the canonical Kohn–Sham orbitals, we calculate the CT numbers of eq 3 averaged over all excitations that fall in the 500−700 nm range and over either the first or last set of frames, that is,

$$\overline{\Omega_{AB}} = \frac{1}{n_{\text{frame}}} \sum_{i=1}^{n_{\text{frame}}} \left(\frac{1}{n_{\text{excitation}}} \sum_{j=1}^{n_{\text{excitation}}} \Omega_{AB}^{j}(i) \right) \tag{13}$$

where $\Omega_{AB}^{j}(i)$ is the CT number Ω_{AB} (calculated according to eq 3) for excitation j in frame i. The resulting average CT number $\overline{\Omega_{AB}}$ is only 11% for the beginning of the trajectory and rises to 40% at the end. This confirms that at the beginning of the simulation, the excitations are mainly composed of local (89%) excitations, with a steep increase in the CT character when the inter-Chl distance drops toward the end of the trajectory.

Although this CT analysis is useful to characterize the nature of the states, it does not directly provide the impact of the change in the CT character on the computed oscillator strengths. For this, we turn to the accompanying analysis of the transition dipole moment contributions. In Table 2, we

Table 2. Average Total Intensity $\overline{f}$ and LE ($\overline{f_{\text{LE}}}$), CT ($\overline{f_{\text{CT}}}$), and OR ($\overline{f_{\text{OR}}}$) Intensity Components of the Total Oscillator Strengths Integrated over an Energy Range of 500−700 nm(and Scaled by 10^{-2}) of the Chla611−Chla612 Pair According to eqs 14 and 15

frames	$\overline{f}$	$\overline{f_{\text{LE}}}$	$\overline{f_{\text{CT}}}$	$\overline{f_{\text{OR}}}$
first set	0.550	0.680	0.111	−0.241
last set	0.354	1.277	0.888	−1.811

decompose the oscillator strengths in the 500−700 nm region according to eq 12. We thereby integrate each component over the energy range of 500−700 nm and average over either the first or the last set of frames of the trajectory.

$$f^{X}(i) = \sum_{j=1}^{n_{\text{excitation}}} f_{j}^{X}(i) \tag{14}$$

$$\overline{f}^{X} = \frac{1}{n_{\text{frame}}} \sum_{i=1}^{n_{\text{frame}}} (f^{X}(i)) \tag{15}$$

We observe that the single-integrated intensity components $f^{\text{LE}}(i)$ and $f^{\text{CT}}(i)$ both increase in magnitude toward the end of

the simulation. As shown in the last column of Table 2, the drop in the total intensity is explained by the orientation factor $f^{\text{OR}}(i)$, defined in eq 12, which depends on the angle between the LE and CT transition dipole moments and can attain both negative and positive values. As shown graphically in Fig.5, where we monitor the value of each of these three terms throughout the 103 frames of the trajectory, during the first part of the simulation (left of the split of the x-axis in Figure 5), the total intensity can be considered as arising largely from the sum of separate local transitions with small corrections due to the mixing of CT states. In the last part (right of the split of the x-axis in Figure 5), this mixing dominates and there is a strong correlation between the magnitude of the terms with the f^{OR} contribution, negating the effect of the increase in f^{LE} and f^{CT}. We also note that the overall decrease in dipole strength is not simply because the CT character increases (as f^{CT} itself is also very large) but because of the destructive interference between LE and CT dipole contributions. It also shows that CT states alone do not necessarily have vanishingly small dipole strength when the distance between the Chls becomes short enough.

■ CONCLUSIONS

We investigated the absorption properties of the Chla611−Chla612 dimer of LHCII using different configurations from two classical molecular dynamics trajectories. Our supra-molecular TDDFT calculations show that a specific dimer configuration, where the two Chls are more stacked and closer to each other, is accompanied by a decrease in the Q-band absorption intensity of about 36% with respect to its initial value. We show that such a decrease can only be predicted if we include CT effects, that is, only if we allow electrons to delocalize between both chromophores. Neglecting CT states, as is done by treating only LE states in a subsystem description, leads to an efficient computational scheme[46,47] but does not capture this effect and should be used with care when chromophores come in close contact. Analysis of the supramolecular transition density matrix in terms of LE and CT components shows that the cause of the decrease is a destructive interference between the transition dipole vectors of the LE and CT states: the individual transition dipoles are increasing, but the orientation of these dipoles is such that the net effect is a decrease in the absorption. Our results indicate that the coupling between LE and CT states should be taken into consideration when deriving parameters for spectral fitting procedures,[43,44] especially for closely interacting pigments. This study highlights the importance of accounting for CT states and electron delocalization when studying the energy landscape of pigment−protein complexes, particularly in the case of strongly interacting pigments. Furthermore, it shows how pigment re-organizations following protein conformational changes can greatly affect the spectral properties. This spectral tunability is fundamental for light-harvesting complexes (LHCs) to be able to switch between different functional states. Previous studies have shown a strong correlation between the LHC energetics and protein conformational changes,[48−50] also showing that the so-called "quenched" states of LHCs are linked to particular conformations where the chromophore−chromophore interactions are strengthened.[39,51−54] In this respect, the Chla611−Chla612 dimer is particularly interesting because it is often assumed to be a critical site for the switch between light-harvesting and quenched conformations of LHCs.[52,55,56]
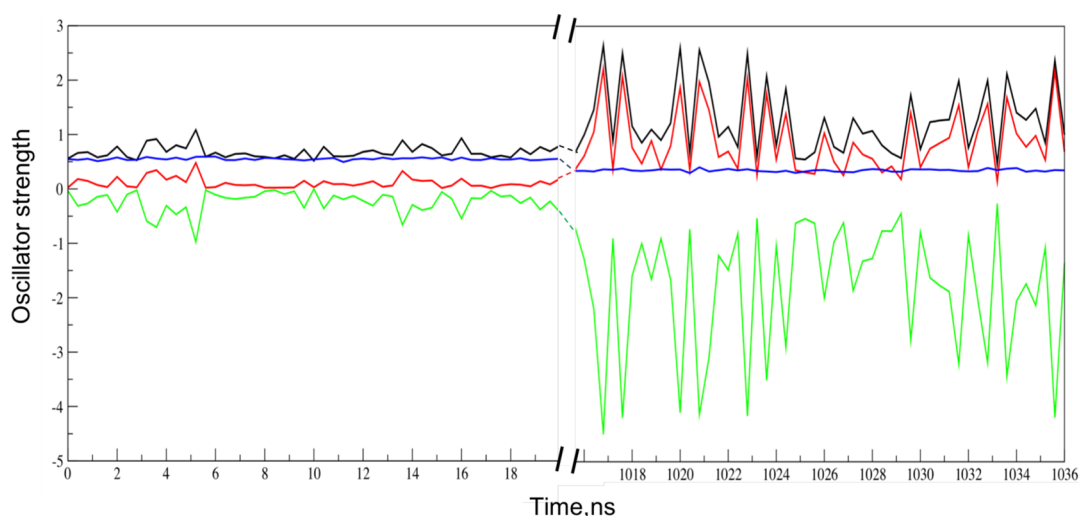
Figure 5. Intensity decomposition according to eq 12 of the Chla611−Chla612 pair during the trajectory. Left and right of the split on the *x*-axis represents the first and last sets of frames from the trajectory "A". For each of the frames, the terms have been integrated over an energy range of 500−700 nm and scaled by 10^{-2}. f^{LE}, f^{CT}, f^{OR}, and the total oscillator strength f are shown in black, red, green, and blue, respectively.

Moreover, an improved knowledge of the nature of these dimer excitations in different orientations can provide hints to help us understand the effects of artificial modifications of the Chla611−Chla612 binding pocket on the overall absorption spectrum of the complex.

ASSOCIATED CONTENT

ⓈⒾ Supporting Information

The Supporting Information is available free of charge at https://pubs.acs.org/doi/10.1021/acs.jpca.1c01467.

> Relative averaged absorption intensities for models (ii), (iii), and (iv) and details of molecular dynamics simulations (PDF)

AUTHOR INFORMATION

Corresponding Author

Lucas Visscher − *Amsterdam Center for Multiscale Modeling, Division of Theoretical Chemistry, Faculty of Sciences, Vrije Universiteit Amsterdam, 1081 HV Amsterdam, The Netherlands;* Ⓞ orcid.org/0000-0002-7748-6243; Email: l.visscher@vu.nl

Authors

Souloke Sen − *Amsterdam Center for Multiscale Modeling, Division of Theoretical Chemistry, Faculty of Sciences, Vrije Universiteit Amsterdam, 1081 HV Amsterdam, The Netherlands*

Vincenzo Mascoli − *Biophysics of Photosynthesis, Dep. Physics and Astronomy, Faculty of Sciences, Vrije Universiteit Amsterdam, 1081 HV Amsterdam, The Netherlands*

Nicoletta Liguori − *Biophysics of Photosynthesis, Dep. Physics and Astronomy, Faculty of Sciences, Vrije Universiteit Amsterdam, 1081 HV Amsterdam, The Netherlands;* Ⓞ orcid.org/0000-0001-5695-4012

Roberta Croce − *Biophysics of Photosynthesis, Dep. Physics and Astronomy, Faculty of Sciences, Vrije Universiteit Amsterdam, 1081 HV Amsterdam, The Netherlands;* Ⓞ orcid.org/0000-0003-3469-834X

Complete contact information is available at:
https://pubs.acs.org/10.1021/acs.jpca.1c01467

Notes
The authors declare no competing financial interest.

ADDITIONAL NOTE

§Residue nomenclature of Liu et al.[2] will be used throughout this article.

REFERENCES

(1) Croce, R.; van Amerongen, H. Light Harvesting in Oxygenic Photosynthesis: Structural Biology Meets Spectroscopy. *Science* **2020**, *369*, No. eaay2058.

(2) Liu, Z.; Yan, H.; Wang, K.; Kuang, T.; Zhang, J.; Gui, L.; An, X.; Chang, W. Crystal Structure of Spinach Major Light- Harvesting Complex at 2.72 Å Resolution. *Nature* **2004**, *428*, 287−292.

(3) Liguori, N.; Croce, R.; Marrink, S. J.; Thallmair, S. Molecular Dynamics Simulations in Photosynthesis. *Photosynth. Res.* **2020**, *144*, 273−295.

(4) Curutchet, C.; Mennucci, B. Quantum Chemical Studies of Light Harvesting. *Chem. Rev.* **2017**, *117*, 294−343.

(5) Andreussi, O.; Prandi, I. G.; Campetella, M.; Prampolini, G.; Mennucci, B. Classical Force Fields Tailored for QM Applications: Is it Really a Feasible Strategy? *J. Chem. Theory Comput.* **2017**, *13*, 4636−4648.

(6) Liguori, N.; Periole, X.; Marrink, S. J.; Croce, R. From Light-Harvesting to Photoprotection: Structural Basis of the Dynamic Switch of the Major Antenna Complex of Plants (LHCII). *Sci. Rep.* **2015**, *5*, 15661.

(7) López-Tarifa, P.; Liguori, N.; van den Heuvel, N.; Croce, R.; Visscher, L. Coulomb Couplings in Solubilised Light Harvesting Complex II (LHCII): Challenging the Ideal Dipole Approximation from TDDFT Calculations. *Phys. Chem. Chem. Phys.* **2017**, *19*, 18311−18320.

(8) Hohenberg, P.; Kohn, W. Inhomogeneous Electron Gas. *Phys. Rev.* **1964**, *136*, B864.

(9) Kohn, W.; Sham, L. J. Self-Consistent Equations Including Exchange and Correlation Effects. *Phys. Rev.* **1965**, *140*, A1133.

(10) Runge, E.; Gross, E. K. U. Density-Functional Theory for Time-Dependent Systems. *Phys. Rev. Lett.* **1984**, *52*, 997.

(11) Casida, M. E. *Recent Advances in Density Functional Methods*; World Scientific: Singapore, 1995; Vol. *1*, p 155.

(12) *Amsterdam Density Functional (ADF)*, v2018; SCM: Amsterdam, The Netherlands, 2001.

(13) Van Gisbergen, S. J. A.; Snijders, J. G.; Baerends, E. J. Implementation of Time-Dependent Density Functional Response Equations. *Comput. Phys. Commun.* **1999**, *118*, 119−138.

(14) Te Velde, G.; Bickelhaupt, F. M.; Baerends, E. J.; Fonseca Guerra, C.; van Gisbergen, S. J.; Snijders, J. G.; Ziegler, T. Chemistry with ADF. *J. Comput. Chem.* **2001**, *22*, 931−967.

(15) Van Der Spoel, D.; Lindahl, E.; Hess, B.; Groenhof, G.; Mark, A. E.; Berendsen, H. J. C. GROMACS: Fast, Flexible, and Free. *J. Comput. Chem.* **2005**, *26*, 1701−1718.

(16) Humphrey, W.; Dalke, A.; Schulten, K. VMD: Visual Molecular Dynamics. *J. Mol. Graphics* **1996**, *14*, 33−38.

(17) RDKit: Open-Source Cheminformatics Software. http://www.rdkit.org (accessed November 2020).

(18) Zapata, F.; Ridder, L.; Hidding, J.; Jacob, C. R.; Infante, I.; Visscher, L. QMflows: A Tool Kit for Interoperable Parallel Workflows in Quantum Chemistry. *J. Chem. Inf. Model.* **2019**, *59*, 3191−3197.

(19) Qmworks: Open-Source Python Library for Workflow Automatisation in Quantum Chemistry Codes. http://www.github.com/SCM-NV/qmworks (accessed November 2020).

(20) *Python Library for Automating Molecular Simulations(PLAMS)*, v2018; SCM: Amsterdam, The Netherlands, 2001.

(21) Pipek, J.; Mezey, P. G. A Fast Intrinsic Localization Procedure Applicable for Ab Initio and Semiempirical Linear Combination of Atomic Orbital Wave Functions. *J. Chem. Phys.* **1989**, *90*, 4916−4926.

(22) Wesolowski, T. A.; Warshel, A. Frozen Density Functional Approach for Ab Initio Calculations of Solvated Molecules. *J. Phys. Chem.* **1993**, *97*, 8050−8053.

(23) Senatore, G.; Subbaswamy, K. R. Density Dependence of the Dielectric Constant of Rare-Gas Crystals. *Phys. Rev. B: Condens. Matter Mater. Phys.* **1986**, *34*, 5754−5757.

(24) Lembarki, A.; Chermette, H. Obtaining a Gradient-Corrected Kinetic-Energy Functional from the Perdew-Wang Exchange Functional. *Phys. Rev. A: At., Mol., Opt. Phys.* **1994**, *50*, 5328.

(25) Becke, A. D. Density-Functional Exchange-Energy Approximation with Correct Asymptotic Behavior. *Phys. Rev. A: At., Mol., Opt. Phys.* **1988**, *38*, 3098.

(26) Lee, C.; Yang, W.; Parr, R. G. Development of the Colle-Salvetti Correlation-Energy Formula into a Functional of the Electron Density. *Phys. Rev. B: Condens. Matter Mater. Phys.* **1988**, *37*, 785.

(27) Jacob, C. R.; Neugebauer, J. Subsystem Density-Functional Theory. *Wiley Interdiscip. Rev.: Comput. Mol. Sci.* **2014**, *4*, 325−362.

(28) Neugebauer, J. Couplings Between Electronic Transitions in a Subsystem Formulation of Time-Dependent Density Functional Theory. *J. Chem. Phys.* **2007**, *126*, 134116.

(29) König, C.; Schlüter, N.; Neugebauer, J. Direct Determination of Exciton Couplings from Subsystem Time-Dependent Density-Functional Theory within the Tamm−Dancoff Approximation. *J. Chem. Phys.* **2013**, *138*, 034104.

(30) Casida, M. E.; Wesołowski, T. A. Generalization of the Kohn−Sham Equations with Constrained Electron Density Formalism and its Time-Dependent Response Theory Formulation. *Int. J. Quantum Chem.* **2004**, *96*, 577−588.

(31) Tölle, J.; Cupellini, L.; Mennucci, B.; Neugebauer, J. Electronic Couplings for Photo-induced Processes from Subsystem Time-Dependent Density-Functional Theory: The Role of the Diabatization. *J. Chem. Phys.* **2020**, *153*, 184113.

(32) Scholz, L.; Tölle, J.; Neugebauer, J. Analysis of Environment Response Effects on Excitation Energies within Subsystem-Based Time-Dependent Density-Functional Theory. *Int. J. Quantum Chem.* **2020**, *120*, No. e26213.

(33) Tölle, J.; Böckers, M.; Niemeyer, N.; Neugebauer, J. Inter-Subsystem Charge-Transfer Excitations in Exact Subsystem Time-Dependent Density-Functional Theory. *J. Chem. Phys.* **2019**, *151*, 174109.

(34) Tölle, J.; Böckers, M.; Neugebauer, J. Exact Subsystem Time-Dependent Density-Functional Theory. *J. Chem. Phys.* **2019**, *150*, 181101.

(35) Plasser, F.; Lischka, H. Analysis of Excitonic and Charge Transfer Interactions from Quantum Chemical Calculations. *J. Chem. Theory Comput.* **2012**, *8*, 2777−2789.

(36) Mayer, I. Charge, Bond Order and Valence in the Ab Initio SCF Theory. *Chem. Phys. Lett.* **1983**, *97*, 270−274.

(37) Milne, B. F.; Toker, Y.; Rubio, A.; Nielsen, S. B. Unraveling the Intrinsic Color of Chlorophyll. *Angew. Chem., Int. Ed.* **2015**, *54*, 2170−2173.

(38) Stockett, M. H.; Musbat, L.; Kjær, C.; Houmøller, J.; Toker, Y.; Rubio, A.; Milne, B. F.; Brøndsted Nielsen, S. The Soret Absorption Band of Isolated Chlorophyll a and b Tagged with Quaternary Ammonium Ions. *Phys. Chem. Chem. Phys.* **2015**, *17*, 25793−25798.

(39) Miloslavina, Y.; Wehner, A.; Lambrev, P. H.; Wientjes, E.; Reus, M.; Garab, G.; Croce, R.; Holzwarth, A. R. Far-red Fluorescence: a Direct Spectroscopic Marker for LHCII Oligomer Formation in Non-Photochemical Quenching. *FEBS Lett.* **2008**, *582*, 3625−3631.

(40) Romero, E.; Mozzo, M.; Van Stokkum, I. H. M.; Dekker, J. P.; Van Grondelle, R.; Croce, R. The Origin of the Low-Energy Form of Photosystem I Light-Harvesting Complex Lhca4: Mixing of the Lowest Exciton with a Charge-Transfer State. *Biophys. J.* **2009**, *96*, L35−L37.

(41) Novoderezhkin, V. I.; Croce, R.; Wahadoszamen, M.; Polukhina, I.; Romero, E.; van Grondelle, R. Mixing of Exciton and Charge-Transfer States in Light-Harvesting Complex Lhca4. *Phys. Chem. Chem. Phys.* **2016**, *18*, 19368−19377.

(42) Ramanan, C.; Ferretti, M.; van Roon, H.; Novoderezhkin, V. I.; van Grondelle, R. Evidence for Coherent Mixing of Excited and Charge-Transfer States in the Major Plant Light-Harvesting Antenna, LHCII. *Phys. Chem. Chem. Phys.* **2017**, *19*, 22877−22886.

(43) Cupellini, L.; Caprasecca, S.; Guido, C. A.; Müh, F.; Renger, T.; Mennucci, B. Coupling to Charge Transfer States is the Key to Modulate the Optical Bands for Efficient Light Harvesting in Purple Bacteria. *J. Phys. Chem. Lett.* **2018**, *9*, 6892−6899.

(44) Nottoli, M.; Jurinovich, S.; Cupellini, L.; Gardiner, A. T.; Cogdell, R.; Mennucci, B. The Role of Charge-Transfer States in the Spectral Tuning of Antenna Complexes of Purple Bacteria. *Photosynth. Res.* **2018**, *137*, 215−226.

(45) Cupellini, L.; Calvani, D.; Jacquemin, D.; Mennucci, B. Charge Transfer from the Carotenoid can Quench Chlorophyll Excitation in Antenna Complexes of Plants. *Nat. Commun.* **2020**, *11*, 662.

(46) Neugebauer, J. Photophysical Properties of Natural Light-Harvesting Complexes Studied by Subsystem Density Functional Theory. *J. Phys. Chem. B* **2008**, *112*, 2207−2217.

(47) König, C.; Neugebauer, J. Quantum Chemical Description of Absorption Properties and Excited-State Processes in Photosynthetic Systems. *ChemPhysChem* **2012**, *13*, 386−425.

(48) Ruban, A. V.; Johnson, M. P.; Duffy, C. D. P. The Photoprotective Molecular Switch in the Photosystem II Antenna. *Biochim. Biophys. Acta, Bioenerg.* **2012**, *1817*, 167−181.

(49) Krüger, T. P. J.; Ilioaia, C.; Johnson, M. P.; Ruban, A. V.; Van Grondelle, R. Disentangling the Low-Energy States of the Major Light-Harvesting Complex of Plants and their Role in Photoprotection. *Biochim. Biophys. Acta, Bioenerg.* **2014**, *1837*, 1027−1038.

(50) Liguori, N.; Roy, L. M.; Opacic, M.; Durand, G.; Croce, R. Regulation of Light Harvesting in the Green Alga Chlamydomonas Reinhardtii: the C-terminus of LHCSR is the Knob of a Dimmer Switch. *J. Am. Chem. Soc.* **2013**, *135*, 18339−18342.

(51) Pascal, A. A.; Liu, Z.; Broess, K.; van Oort, B.; van Amerongen, H.; Wang, C.; Horton, P.; Robert, B.; Chang, W.; Ruban, A. Molecular Basis of Photoprotection and Control of Photosynthetic Light-Harvesting. *Nature* **2005**, *436*, 134−137.

(52) Ruban, A. V.; Berera, R.; Ilioaia, C.; Van Stokkum, I. H. M.; Kennis, J. T. M.; Pascal, A. A.; Van Amerongen, H.; Robert, B.; Horton, P.; Van Grondelle, R. Identification of a Mechanism of

Photoprotective Energy Dissipation in Higher Plants. *Nature* **2007**, *450*, 575−578.

(53) Ahn, T. K.; Avenson, T. J.; Ballottari, M.; Cheng, Y.-C.; Niyogi, K. K.; Bassi, R.; Fleming, G. R. Architecture of a Charge-Transfer State Regulating Light Harvesting in a Plant Antenna Protein. *Science* **2008**, *320*, 794−797.

(54) Bode, S.; Quentmeier, C. C.; Liao, P.-N.; Hafi, N.; Barros, T.; Wilk, L.; Bittner, F.; Walla, P. J. On the Regulation of Photosynthesis by Excitonic Interactions between Carotenoids and Chlorophylls. *Proc. Natl. Acad. Sci. U.S.A.* **2009**, *106*, 12311−12316.

(55) Mozzo, M.; Passarini, F.; Bassi, R.; van Amerongen, H.; Croce, R. Photoprotection in Higher Plants: the Putative Quenching Site is Conserved in all Outer Light-Harvesting Complexes of Photosystem II. *Biochim. Biophys. Acta, Bioenerg.* **2008**, *1777*, 1263−1267.

(56) Mascoli, V.; Liguori, N.; Xu, P.; Roy, L. M.; van Stokkum, I. H. M.; Croce, R. Capturing the Quenching Mechanism of Light-Harvesting Complexes of Plants by Zooming in on the Ensemble. *Chem* **2019**, *5*, 2900−2912.

■ NOTE ADDED AFTER ASAP PUBLICATION

Due to a production error, this article originally published with errors in the header columns of Table 2. The headers were corrected and the article reposted May 27, 2021.